

# Fractionalized conductivity and emergent self-duality near topological phase transitions

Yan-Cheng Wang,<sup>1</sup> William Witczak-Krempa,<sup>2,3</sup> Meng Cheng,<sup>4</sup> and Zi Yang Meng<sup>5,\*</sup>

<sup>1</sup>*School of Materials Science and Physics, China University of Mining and Technology, Xuzhou 221116, China*

<sup>2</sup>*Département de physique, Université de Montréal Montréal (Québec), H3C 3J7, Canada*

<sup>3</sup>*Centre de Recherches Mathématiques, Université de Montréal; P.O. Box 6128, Centre-ville Station; Montréal (Québec), H3C 3J7, Canada*

<sup>4</sup>*Department of Physics, Yale University, New Haven, CT 06520-8120, U.S.A*

<sup>5</sup>*Department of Physics and HKU-UCAS Joint Institute of Theoretical and Computational Physics, The University of Hong Kong, Pokfulam Road, Hong Kong SAR, China*

(Dated:)

## Abstract

The experimental discovery of the fractional Hall conductivity in two-dimensional electron gases revealed new types of quantum particles, called anyons, which are beyond bosons and fermions as they possess fractionalized exchange statistics. These anyons are usually studied deep inside an insulating topological phase. It is natural to ask whether such fractionalization can be detected more broadly, say near a phase transition from a conventional to a topological phase. To answer this question, we study a strongly correlated quantum phase transition between a topological state, called a  $\mathbb{Z}_2$  quantum spin liquid, and a conventional superfluid using large-scale quantum Monte Carlo simulations. Our results show that the universal conductivity at the quantum critical point becomes a simple fraction of its value at the conventional insulator-to-superfluid transition. Moreover, a dynamically self-dual optical conductivity emerges at low temperatures above the transition point, indicating the presence of the elusive vison particles. Our study opens the door for the experimental detection of anyons in a broader regime, and has ramifications in the study of quantum materials, programmable quantum simulators, and ultra-cold atomic gases. In the latter case, we discuss the feasibility of measurements in optical lattices using current techniques.

## Introduction

Correlated topological phases exhibit phenomena that extend beyond the conventional paradigms of condensed matter physics, namely Landau's Fermi liquid theory for metals and the Landau-Ginzburg-Wilson symmetry breaking scheme for phases and transitions. These topological phases are the embodiment of intrinsic topological order [1], and call for a deeper understanding of states of matter. Topologically ordered systems exhibit new types of particles called anyons that are neither fermions nor bosons. Some of these anyons can be used to robustly encode and manipulate quantum information, thus offering a viable platform for quantum computation [2].

Topological order was experimentally discovered in two-dimensional electron gases (2DEGs) under strong

magnetic fields by measuring a well-known observable: the Hall conductivity. In the simplest integer quantum Hall state, the Hall conductivity is universally quantized as  $\sigma_{xy} = e^2/h$ , where  $e$  is the electron charge and  $h$  Planck's constant. In contrast, in fractional quantum Hall states [3, 4],  $\sigma_{xy}$  remains universal but becomes a fraction of  $e^2/h$  as a consequence of the fractionalization of the electron. One prominent example is the fractional Hall state with  $\sigma_{xy} = \frac{1}{3} \frac{e^2}{h}$  where the electrons fractionalize into anyons of charge  $e/3$ . Subsequent experiments, such as shot noise analysis of the edge modes [5, 6], and thermal Hall conductance [7] have confirmed the fractionalized nature of the excitations. Unfortunately, many other equally interesting topologically ordered systems do not possess a universal Hall response, nor robust edge states. A representative example is the  $\mathbb{Z}_2$  quantum spin liquid QSL, or in the boson language, topologically ordered insulator [8], which could arise in frustrated magnets, bosonic Mott insulators or Rydberg atom based programmable quantum simulators [9–15]. Unlike a regular paramagnet that would host bosonic spin waves, this spin liquid has emergent bosonic and fermionic excitations, which carry  $1/2$  of the spin quanta of the spin waves, as well as visons, which are fluxes of an emergent gauge field. As the fluxes can only take two inequivalent values, the gauge field is said to be of  $\mathbb{Z}_2$  type. A continuous transition between such a state and a conventional one is bound to be beyond the usual Landau-Ginzburg-Wilson paradigm. Direct experimental detection of fractionalization in these systems has remained an outstanding challenge [16–20].

Here, we propose a new experimental signature for fractionalization in  $\mathbb{Z}_2$  QSLs that can be obtained already at the transition point from a conventional phase. As a concrete example, we consider a system in proximity to a quantum critical transition from a  $\mathbb{Z}_2$  QSL to an ordinary superfluid, as shown in Fig. 1. Despite being gapless, the system's longitudinal conductivity becomes a simple fraction,  $1/4$ , of its value at the usual quantum critical point between a trivial paramagnet and a superfluid. This fraction is a direct consequence of the fractionalization of the charge carriers at the quantum

critical point (QCP), which carry  $1/2$  of the unit charge of the microscopic bosons. “Charge” here refers to the boson number (or spin, in a Mott insulator of electrons), so the bosons effectively split in two at the transition and in the quantum spin liquid, which is illustrated schematically in Fig. 1 (b). In addition, we uncover a crossover from a particle-like dynamical conductivity at low temperature, to a vortex-like one at higher temperatures. At an intermediate temperature denoted by  $T_*$ , the dynamical conductivity becomes nearly frequency-independent signalling the emergence of self-dual quantum fluid. We argue that this striking behavior reveals the presence of visons, which are otherwise challenging to observe as they do not carry charge (spin). In the Discussion, we argue that these signatures can be observed using existing techniques in ultra-cold atomic gases loaded in an optical kagome lattice.

## Results

**Topological phase transition on the kagome lattice.** We consider the following Balents-Fisher-Girvin (BFG) model for bosons on a kagome lattice [9–14], depicted in Fig. 1 (a):

$$H = -t \sum_{\langle ij \rangle} \left( b_i^\dagger b_j + \text{h.c.} \right) - \mu \sum_i n_i + V \left( \sum_{\langle ij \rangle} n_i n_j + \sum_{\langle\langle ij \rangle\rangle} n_i n_j + \sum_{\langle\langle\langle ij \rangle\rangle\rangle} n_i n_j \right) \quad (1)$$

where  $b_i^\dagger$  ( $b_i$ ) creates (annihilates) a hard-core boson at site  $i$ , and  $n_i = b_i^\dagger b_i$  measures the number of bosons therein. The  $t$  term hops bosons between neighboring sites and the  $V$  terms are repulsive interactions between any two bosons on a hexagon, see Fig. 1 (a). By the mapping  $b_i^\dagger(b_i) \rightarrow S_i^+(S_i^-)$ , and  $n_i - 1/2 \rightarrow S_i^z$ , the Hamiltonian can also be cast into an XXZ spin model, with the chemical potential  $\mu$  corresponding to external magnetic field  $h$ . We work primarily at the filling factor of  $\langle n_i \rangle = 1/2$ , i.e.,  $1/2$  bosons at every site on average. The  $\langle n_i \rangle = 1/3$  filling will be discussed below, and in that case, another repulsion  $V'$  between the same sublattice sites on the neighboring hexagons is added to stabilize the QSL phase [13]. The Hamiltonian (1) conserves the total number of bosons, which corresponds to a  $U(1)$  symmetry. Accordingly,  $b_i^\dagger$  creates an excitation of charge 1, which is the fundamental unit of charge in the system, in analogy with the charge of an electron in a solid.

As shown in Fig. 1 (b), at large  $t/V$ , the bosons can hop freely and will Bose-Einstein condense to form a superfluid at low temperature. In contrast, when the repulsion dominates an insulator will result, in which case the bosons become effectively frozen. Large-scale quantum Monte Carlo (QMC) simulations have shown that this quantum phase transition occurs at  $(t/V)_c =$

$0.070756(20)$  [10, 12]. So far, these properties seem conventional. However the striking feature is that the insulator is a topological state of matter with fractionalized particles. Indeed, the emergent excitations do not carry charge 1 as expected, but rather  $1/2$ : they are heuristically speaking half-bosons. The charge 1 bosons become fractionalized into pairs of bosons (called spinons) with half the fundamental charge. This is the analog of emergent charge  $e/3$  particles in a fractional quantum Hall state at filling  $1/3$ . In fact, there are three types of topologically nontrivial emergent quasiparticles in the  $\mathbb{Z}_2$  QSL: a bosonic spinon which carries half-integer charge, a bosonic vison with integer charge (including zero) but carrying  $\pi$  flux of the emergent  $\mathbb{Z}_2$  gauge field, and their bound state – a fermionic spinon.

Furthermore, the quantum phase transition itself is highly unconventional. While it can be intuitively understood as the Bose-Einstein condensation transition of bosonic spinons, the symmetry breaking paradigm of Landau-Ginzburg cannot explain the emergent fractionalization. Interestingly, the transition is continuous meaning that quantum critical fluctuations proliferate to large scales, and can thus amplify signatures of fractionalization.

Using large-scale quantum Monte Carlo (QMC) simulations we search for such signatures using a key observable, the conductivity. This is in part motivated by the fundamental role that the conductivity has played in the discovery of fractional quantum Hall states. Since time-reversal is not broken here, the Hall conductivity vanishes and we are left with the longitudinal conductivity, denoted by  $\sigma$ . One couples the system to an external potential that causes a flow of charge (bosons), and the conductivity is given by the linear response expression  $\sigma(\omega) = -\frac{i}{\omega} \langle J_x(\omega) J_x(-\omega) \rangle$ , where we have allowed for a drive oscillating with frequency  $\omega$ . In the Discussion, we explain how this is possible using current techniques in ultra-cold atomic gases.  $J_x(\omega)$  is the usual boson current along the  $x$ -direction (denoted by the lattice vector  $\mathbf{r}_1$  in Fig. 1 (a)) at frequency  $\omega$ . In the QMC simulations, one has directly access to imaginary frequencies  $\omega \rightarrow i\omega_n = i2\pi Tn$ , where  $n$  is an integer and  $T$  the temperature. An important challenge is the continuation from imaginary to real frequencies. Reliable numerical techniques for this purpose, such as stochastic analytic continuation [21, 22] which we will use in this work, are under active development and have been successfully employed in various quantum many-body systems [14, 23–25].

In Fig. 2, we show the conductivity of the system at the quantum critical coupling  $(t/V)_c = 0.070756(20)$  and filling  $\langle n_i \rangle = 1/2$ . We compute  $\sigma(\omega_n)$  with system sizes  $L = 12, 24, 36, 48, 60, 72, 96$  and inverse temperature  $\beta V = 300, 350, 390, 400, 450, 500, 600$  (with statistical errors obtained from QMC simulations and standard data fitting; this also applies to the data shown in Fig. 3)).

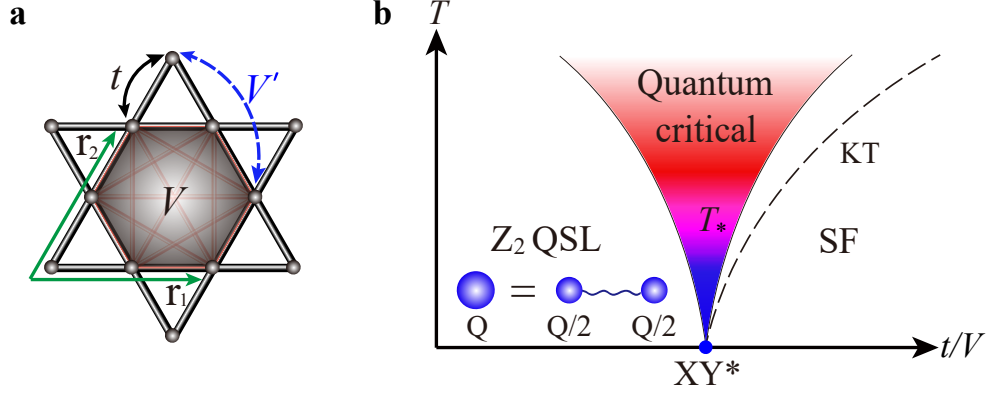


**Fig. 1. Kagome model for a topological phase transition.** **a** Kagome lattice with lattice vectors  $\mathbf{r}_{1,2}$ . The hopping  $t$  and the interaction  $V$  are given in the Hamiltonian Eq. (1). **b** Phase diagram of the kagome model as a function of  $t/V$ , and temperature  $T$ . The  $Z_2$  quantum spin liquid (QSL), superfluid (SF), and the XY\* quantum critical point characterizing the groundstate are shown. The charge fractionalization of spinons is schematically illustrated. In the quantum critical fan, blue indicates a particle-like conductivity, while an unconventional vortex-like response is in red. A nearly self-dual dynamical conductivity emerges at intermediate temperatures (purple) signaling the presence of visons. The same color scheme is used in representing the conductivity data in Figs. 2-3. The SF long-range order only exists at zero temperature; a Kosterlitz-Thouless (KT) transition, denoted by the black dashed line, separates the paramagnetic phase from the one with quasi-long-range order.

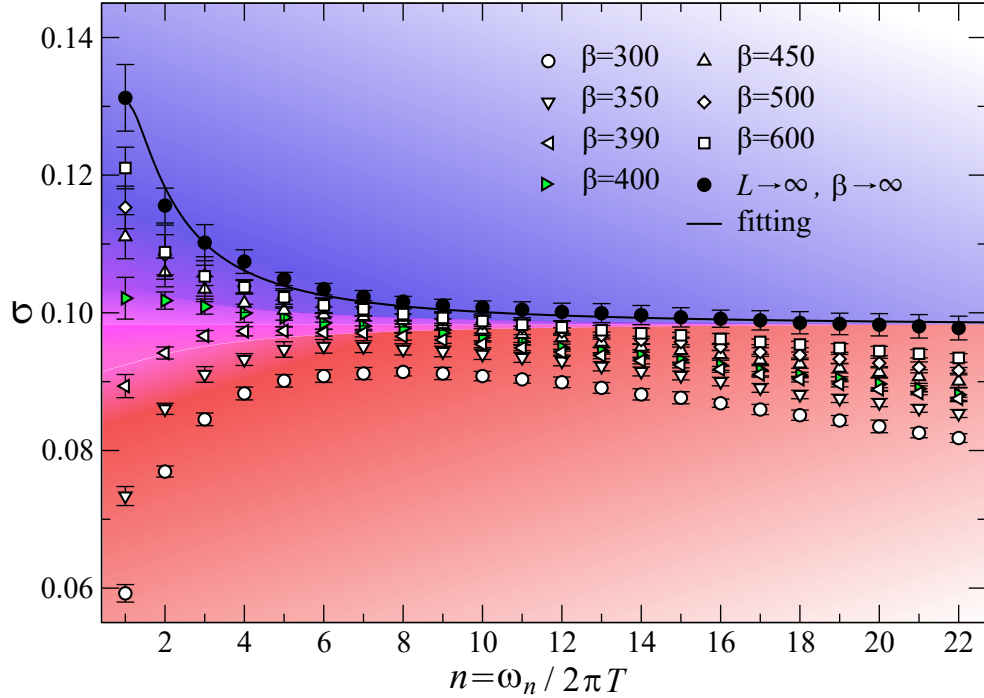


**Fig. 2. Conductivity fractionalization and dynamical self-duality at half-filling.** Longitudinal conductivity data, including a two-step extrapolation from finite sizes and temperatures to the low- $T$  thermodynamic limit, of our kagome model at boson filling  $\langle n_i \rangle = 1/2$  as a function of  $n = \omega_n / 2\pi T$  at the XY\* critical point  $(t/V)_c = 0.070756(20)$  with  $L = 12, 24, 36, 48, 60, 72, 96$  and  $\beta V = 300, 350, 390, 400, 450, 500, 600$ . In the thermodynamic limit,  $L \rightarrow \infty$  and then  $\beta \rightarrow \infty$ , the universal constant  $\sigma_{XY^*}(\infty)$  appears, and we obtain a plateau value of  $\sigma_{XY^*}(\infty) = 0.098(9)$  which is  $\frac{1}{4}\sigma_{XY}(\infty)$ . At finite temperatures, we see crossover from a particle-like conductivity (blue) to a vortex-like one (red). In the vicinity of  $\beta_* \approx 400$  (c.f. the green triangles), we observe a nearly constant dynamical conductivity indicating a self-dual quantum fluid with visons.

QMC simulations and conductivity measurements are described in the Methods section, and additional details, especially the two-step extrapolation of  $\sigma(L \rightarrow \infty, \beta \rightarrow \infty)$  to the thermodynamic limit, are given in the Supplementary Note 2. We plot the finite temperature conductivity and extrapolate them to the  $L \rightarrow \infty$  and then  $\beta \rightarrow \infty$  ( $T \rightarrow 0$ ) limit, as shown by the black solid dots, and  $\sigma$  is then expected to become a universal scaling function of  $f(\omega/T)$ , or in imaginary frequencies,  $f(i\omega_n/T)$  [26, 27]. In the low temperature regime  $\omega_n \gg T$ , the conductivity should saturate to its groundstate constant value  $\sigma(\infty)$ . This plateau is clearly observed in Fig. 2, and the resulting conductivity obeys a striking relation:

$$\sigma_{XY^*}(\infty) = \frac{1}{4} \sigma_{XY}(\infty), \quad (2)$$

where XY denotes the conventional superfluid-to-insulator transition which is of the XY universality, and since the transition in our model involves fractionalization, it is denoted as XY\* [9, 28, 29]. The XY transition arises in non-frustrated lattices, the canonical example being the Bose-Hubbard model on the square lattice at unit filling, which has been experimentally realized with ultra-cold atoms [30]. Comparing our numerical value  $\sigma_{XY^*}(\infty) = 0.098(9)$  with the best estimate for that of the XY transition  $\sigma_{XY} = 0.3554$  [31–36] gives a ratio  $\sigma_{XY^*}(\infty)/\sigma_{XY}(\infty) = 0.27(3)$ , which is  $1/4$  within error bars. The suppression of the conductivity at the fractionalized XY\* critical point compared to its XY counterpart is given by a simple rational number,  $1/4$ , which is reminiscent of the fractional Hall conductivity observed in 2DEGs – also a rational fraction of the conductivity at unit filling.

We now turn to the case of  $\langle n_i \rangle = 1/3$  filling. It was shown in Ref. [13] that a XY\* QCP also occurs between  $\mathbb{Z}_2$  QSL and superfluid phases, when the aforementioned  $V'$  term is added to the Hamiltonian to stabilize the QSL. The  $\mathbb{Z}_2$  QSL in this case has identical topological order as the one at  $1/2$  filling, and spinons still carry half U(1) charge [12, 14, 20]. Although the emergent  $\mathbb{Z}_2$  gauge field sees a different background charge density for  $1/2$  and  $1/3$  fillings, we expect this subtle difference do not affect the critical properties at the XY\* transition. The QMC results are shown in Fig. 3, with system sizes  $L = 12, 24, 36, 48, 60, 72$ , and  $\beta V = 400, 450, 500, 520, 550, 600$  at the critical point  $(t/V)_c = 0.07773(5)$ . The plateau in the conductivity, after the two-step extrapolation to the thermodynamic limit (as denoted by the black solid dots), also yields  $\sigma_{XY^*}(\infty) = 0.100(13)$  and  $\sigma_{XY^*}(\infty)/\sigma_{XY} = 0.28(4)$ , which is again  $\frac{1}{4}$  within error bars.

As we shall now explain, the fractionalized conductivity observed here and the fractional Hall conductivity observed in 2DEGs share a common origin: charge fractionalization.

**From fractionalized charge to fractional conductivity.** To understand the aforementioned results at the XY\* QCP, we can resort to a coarse-grained description in terms of a quantum field theory. A complex field  $\phi$  is introduced to represent the emergent bosonic spinons. Since a conventional charge 1 boson is associated with a pair of spinons, we assign a unit charge to  $\phi^2$ . As such, the spinon field must carry charge  $Q = 1/2$  under the U(1) particle conservation symmetry. The form of the Hamiltonian is then constrained by the fact that the critical theory has an emergent Lorentz invariance and takes the same form as for the regular XY transition:  $H = \int d^2\mathbf{x} (|\partial_0 \phi|^2 + |\nabla \phi|^2 + r|\phi|^2 + \lambda|\phi|^4)$ , where  $r$  tunes the system to criticality. It is important to note that physical observables must be composed of an even number of spinons. For instance, the superfluid corresponds to a Bose-Einstein condensate of conventional bosons, namely  $\phi^2$ . Since we are interested in the conductivity, we need to first specify the form of the physical current:

$$\mathbf{J} = \frac{1}{2} i(\phi \nabla \phi^* - \phi^* \nabla \phi) \quad (3)$$

which is  $1/2$  of the usual current one would get at the XY transition. The  $1/2$  ensures that the field describing the original bosons has a unit U(1) charge. It then follows from the linear response expression  $\sigma = -\frac{i}{\omega} \langle J_x(\omega) J_x(-\omega) \rangle$  that the conductivity at the XY\* transition is  $1/4$  that of its XY value, in perfect agreement with our numerical results, i.e., both at the XY\* QCPs of  $\langle n_i \rangle = 1/2$  in Fig. 2 and  $\langle n_i \rangle = 1/3$  in Fig. 3. We note that the above argument is non-perturbative in the interaction strength since the  $\mathbb{Z}_2$  gauge field, and the associated gapped visons, become non-dynamical at asymptotically low temperatures.

**Visons and dynamical self-duality.** Besides probing the groundstate at the quantum phase transition, our results for the conductivity shown in Figs. 2-3 extend well into the quantum critical fan of Fig. 1 (b) at finite temperature. This experimentally accessible regime offers an opportunity to probe strongly interacting quantum fluids in thermal equilibrium. Due to the emergent scale invariance at quantum criticality, the rate for excitations to relax is given by the absolute temperature  $k_B T/\hbar$  [37], where we have temporarily reinstated Boltzmann's and Planck's constants. As such, the finite frequency conductivity will be a scaling function of the frequency divided by this universal rate,  $\sigma(\omega, T) = f(\omega/T)$ , which holds at sufficiently low  $T$  but for fixed  $\omega/T$ . We have obtained this universal scaling function at imaginary frequencies  $f(i\omega_n/T)$ , see the fit of the thermodynamic values in Figs. 2-3 (the fitting procedure is described in the Supplementary Note 2). At large values of the argument,  $f(i\omega_n/T)$  reduces to the groundstate conductivity, which is  $1/4$  the value of the ordinary XY QCP.

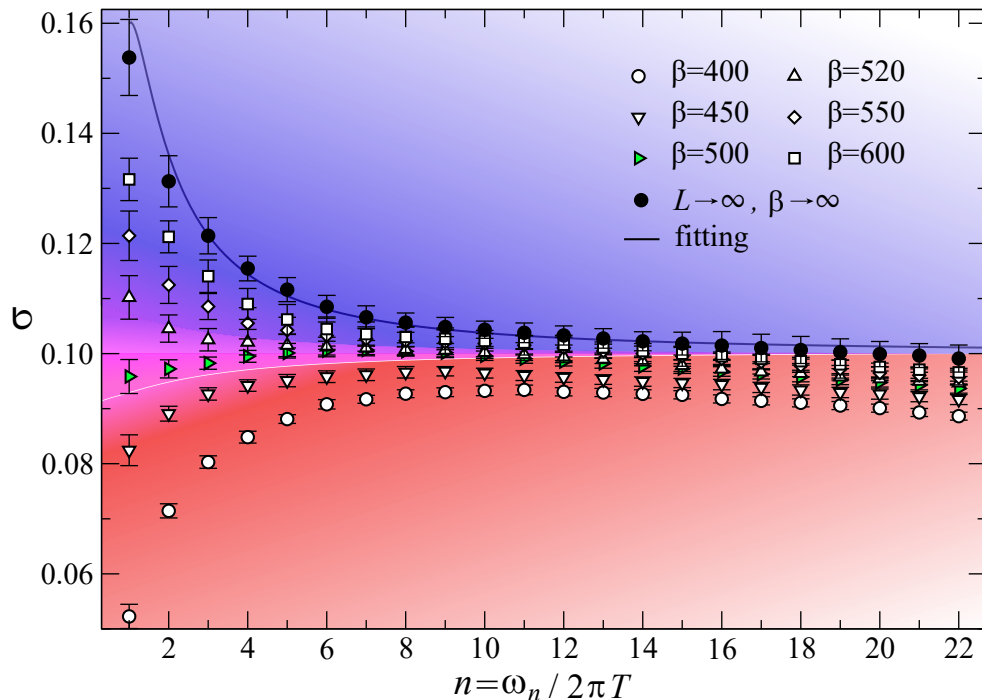


**Fig. 3. Topological signatures at 1/3 filling.** The conductivity data of our kagome lattice model at boson filling  $\langle n_i \rangle = 1/3$  as a function of  $n = \omega_n / 2\pi T$  at the XY\* critical point  $(t/V)_c = 0.07773(5)$ , with  $V'/V = 0.005$ ,  $L = 12, 24, 36, 48, 60, 72$  and  $\beta V = 400, 450, 500, 520, 550, 600$ . In the thermodynamic limit  $L \rightarrow \infty$  and then  $\beta \rightarrow \infty$ , the universal constant  $\sigma_{XY^*}(\infty)$  appears, and we obtain  $\sigma_{XY^*}(\infty) = \frac{1}{4}\sigma_{XY}(\infty)$  as discussed in the text. As in Fig. 2, we see a thermal crossover from a particle-like conductivity (blue) to a vortex-like one (red). The self-dual regime occurs around  $\beta_* \approx 500$  (c.f. the green triangles).

At smaller frequencies, the scaling function shows the same upturn previously obtained using QMC simulations for the regular XY QCP [31–35]. A response with such an upturn is referred to as particle-like [20, 38, 39] since it shares the same form as that of regular bosons in the XY universality class. In Figs. 2-3, we observe that as the quantum system is heated up, there is a gradual reduction of the upturn of the low-frequency conductivity. At sufficiently high temperatures, the conductivity acquires a downturn near the DC limit. We say that such a conductivity is the “dual” of the particle-like conductivity since under the usual particle-vortex duality, the dual vortices have a conductivity given by the inverse of that of the original bosons,  $1/\sigma(\omega)$  [40]. The duality thus converts an upturn into a downturn, yielding a vortex-like conductivity [38, 39]. At an intermediate temperature that we call  $T_*$ , the dynamical conductivity becomes nearly frequency-independent as is shown in purple in Figs. 2-3. We refer to this type of conductivity as dynamically self-dual owing to the fact that under usual particle-vortex duality, a frequency-independent response remains flat [41]. This crossover from particle-like to vortex-like response within the quantum critical fan results from the geometrical frustration of the kagome Hamiltonian, and is absent at the conventional XY tran-

sition [31]. It is thus a striking new feature of the topological phase transition.

In order to understand the origin of this striking phenomenon, we need to go back to the full cast of topological particles. Beyond the spinons described by the XY\* field theory discussed above, the QSL also hosts charge-neutral visons [20]. As these are gapped, they decouple at asymptotically low temperatures. However, as we heat the system, the temperature approaches the gap scale of the visons, which we shall independently quantify below. The visons then become thermally excited, and begin to interact and scatter the charge-carrying spinons. This new scattering channel leads to the observed reduction of the conductivity at low frequencies. As the visons are  $\pi$ -fluxes of the emergent gauge field, the spinons effectively move in a random background emergent magnetic field, which results in lower mobility. Remarkably, the dynamical conductivity in the self-dual regime is  $\sigma(\omega) \approx \frac{1}{4}\sigma_{XY}(\infty)$  for all frequencies, extending the topological fractionalization to the dynamical regime. It is important to emphasize that we have written the conductivity in real frequencies since the analytic continuation can be trivially performed for a constant function, which is an advantage of the self-dual regime compared to temperatures away from  $T_*$ .

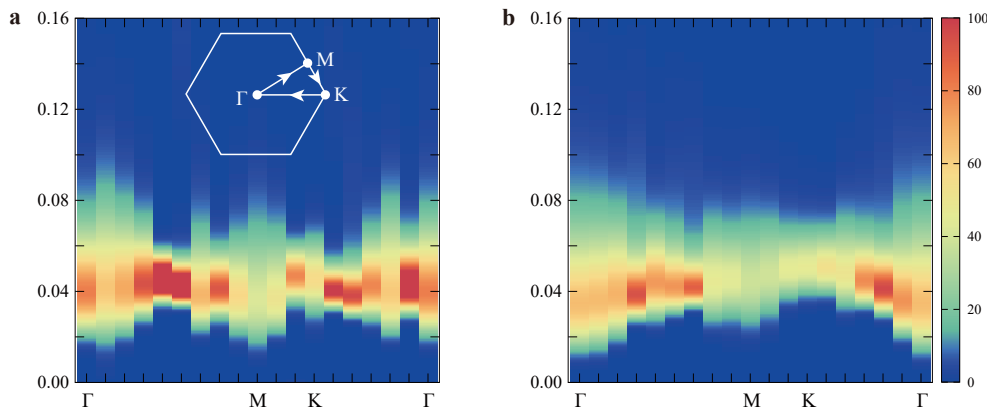


**Fig. 4. Probing the vison gap.** Vison-pair spectra obtained from the QMC dynamical density-density  $\langle n_i(\tau)n_j(0) \rangle$  (or  $\langle S_i^z(\tau)S_j^z(0) \rangle$  in the spin language) correlation function and stochastic analytic continuation, plotted along the high symmetry path  $\Gamma$ - $M$ - $K$ - $\Gamma$  in the Brillouin zone. The horizontal axis is momentum, while the vertical one represents energy (frequency) (note the energy scale here is very low compared with, for example, the scale of the bare interaction which is  $V = 1$ ). **a** At the  $XY^*$  critical point  $(t/V)_c = 0.070756$  at boson filling  $\langle n_i \rangle = 1/2$  with system size  $L = 18$  and  $\beta = 500$ . **b** At the  $XY^*$  critical point  $(t/V)_c = 0.07773$  at filling  $\langle n_i \rangle = 1/3$  with system size  $L = 18$  and  $\beta = 600$ . The vison-pair continua are clearly visible above (twice) the vison gap.

To further test the above conclusion regarding the vison signatures in the conductivity, we analyze the QMC dynamical density-density correlation function  $\langle n_i(\tau)n_j(0) \rangle$  (or  $\langle S_i^z(\tau)S_j^z(0) \rangle$  in the spin language), and stochastically analytically continue to real frequencies [14, 22–24]. We expect the number density correlations to reveal properties about vison excitations, as deep inside the spin liquid phase ( $t/V \ll 1$ ) it can be shown that the number operator  $n_i$  (or  $S_i^z$ ) creates a pair of visons [9, 14]. The vison gap should stay finite within the entire spin liquid phase, including the QCP, so it is reasonable to expect that  $n_i$  creates vison pairs near and at the transition. Fig. 4 (a) shows the spectrum for filling 1/2, while Fig. 4 (b) is for filling 1/3. A fundamental feature of the spectra is the absence of excitations at low energies, which leads to the conclusion that the visons are gapped [14]. We have also verified the vison gap by directly measuring the exponential decay of the  $\langle S_i^z(\tau)S_j^z(0) \rangle$  correlation in imaginary time QMC data, and the obtained gaps are consistent with those read from the spectra in Fig. 4 (examples of the comparison are given in the Supplementary Note 3). The gap in the spectrum gives twice the vison gap  $\Delta_v$ , since visons are always created in pairs. We thus estimate  $\Delta_v \sim 0.01$  at filling 1/2, and  $\sim 0.005$  at filling 1/3. We expect that  $\Delta_v$  sets the scale for the self-dual temperature  $T_*$  obtained for the conductivity. We indeed find that these two quantities are of the same order of magnitude, with  $T_*$  being roughly a third of the vison gap. Furthermore,  $\Delta_v$  is lower at 1/3 filling compared to half filling, consistent with the fact that  $T_*$  is smaller at 1/3 filling. It would be interesting to perform a more detailed theoretical analysis that would relate  $T_*$  to the vison gap. This would require studying a field theory beyond the one for

the pure  $XY^*$  quantum critical point, since finite mass visons would need to be included at finite temperature.

## Discussion

We obtained the finite frequency conductivity near the unconventional  $XY^*$  quantum critical point, which is associated with fractionalization, topological order and an emergent  $\mathbb{Z}_2$  gauge field. The topological phase transition separates a  $\mathbb{Z}_2$  QSL harboring fractionalized spinon and vison excitations from a conventional superfluid phase. We have shown that the groundstate conductivity reveals the existence of fractionalized charge, i.e.  $\sigma_{XY^*}(\infty) = \frac{1}{4}\sigma_{XY}(\infty)$ . This sharp signature in the conductivity is to be contrasted with other types of “indirect” measurements on QSLs such as inelastic neutron scattering that can only observe the spinon-pair continua, which is easily confused with the continua generated from disorder [42, 43]. We have uncovered another qualitatively new signature, namely the crossover from a particle-like (DC upturn) to a vortex-like (DC downturn) dynamical conductivity as the system is heated up. Strikingly, at intermediate temperatures we discovered a dynamically self-dual conductivity that is nearly independent of the frequency  $\sigma(\omega) \approx \frac{1}{4}\sigma_{XY}(\infty)$ . This is in sharp contrast to the usual XY transition, and results from the presence of thermally excited topological particles, the visons. Therefore, the conductivity fractionalization and emergent self-duality discovered in this work open the door for the experimental detection of fractionalized particles such as anyons in a variety of quantum materials, and ultra-cold atomic gases for example the recently proposed Rydberg atom based programmable quantum simulators on the kagome lattice [15]. Recent experiments [47] in ultra-cold atomic gases have yielded the

frequency-dependent conductivity for atoms loaded in a two-dimensional optical lattice, which is precisely what is needed to measure the conductivity predicted in our work. In the experiment, the alternating current is obtained by applying a spatially uniform but temporally oscillating force via the displacement of a harmonic trapping potential. Since we predict the emergence of a dynamically self-dual regime, this should be easier to observe since it will be apparent in a wide range of frequencies, and does not require that the system be cooled to the absolute lowest temperatures. We reiterate that the self-dual response holds at real frequencies, which is what is measured. We also note that bosonic atoms have been successfully loaded in an optical kagome lattice [48], so that all the basic experimental ingredients are present. Finally, it will be of interest to extend our findings to other QSL phases, as well as to certain non-Fermi liquids and their unconventional transitions. As a concrete example, it would be of interest to study the finite-temperature dynamical conductivity near the topological QCP that is “dual” to the one studied in this work: visons condense, while the spinons maintain a small gap throughout. An inversion of the observed crossover would be expected, since the vison gap is very small in our system, one can certainly design other lattice models hosting  $\mathbb{Z}_2$  QSL with comparable spinon and vison energy scales [20], but a detailed study is needed owing to the strongly interacting nature of the transition.

## Methods

We simulate the Hamiltonian in Eq. (1) on the kagome lattice by using a worm-type continuous time QMC technique [44, 45]. In the simulations, we take system sizes  $L = 12, 24, 36, 48, 60, 72, 96$ , and the inverse temperature  $\beta V = 300, 350, 400, 450, 500, 520, 550, 600$ . The conductivity  $\sigma$  can be expressed as  $\sigma(i\omega_n) = -\frac{i}{\omega_n} \langle J_x(\omega_n) J_x(-\omega_n) \rangle$  with  $J_x(\omega_n)$  the current operator along the  $x$ -direction ( $\mathbf{r}_1$  in Fig. 1 (a)) of the kagome lattice. In the QMC simulations, the imaginary frequency conductivity  $\sigma(i\omega_n)$  is computed as

$$\begin{aligned} \sigma(i\omega_n) &= \frac{\langle -k_x \rangle - \Lambda_{xx}(i\omega_n)}{\omega_n} \\ &= \frac{\langle |\sum_k P_k^x e^{i\omega_n \tau_k}|^2 \rangle}{\beta L^2 \omega_n} \end{aligned} \quad (4)$$

where  $\langle k_x \rangle$  is the kinetic energy associated with the  $x$ -oriented bond, and  $\Lambda_{xx}(i\omega_n)$  is the fourier transform of imaginary time current-current correlation function [46], and  $\sum_k$  runs through the volume of  $L \times L \times \beta$  of the QMC configurational space with  $P_k^x$  denoting the projection of the  $k$ -th hopping along the  $x$ -direction. Similar measurement of conductivity has been performed at the XY QCP [33].

In order to obtain real-frequency spectral functions, the stochastic analytic continuation (SAC) scheme is employed to obtain the spectral function  $A(\mathbf{q}, \omega)$  from the

imaginary-time correlation function  $S(\mathbf{q}, \tau)$ ,  $S(\mathbf{q}, \tau) = \frac{1}{\pi} \int_0^\infty d\omega A(\mathbf{q}, \omega) (e^{-\tau\omega} + e^{-(\beta-\tau)\omega})$ . It is known that the problem of inverting the Laplace transform is equivalent to find the most probable spectra  $A(\omega)$  out of its exponentially many suggestions to match the QMC correlation function  $S(\tau)$  with respect to its stochastic errors, and such transformation has been converted to a Monte Carlo sampling process [21, 22]. This QMC-SAC approach has been successfully applied to quantum magnets ranging from the simple square lattice Heisenberg antiferromagnet [23, 25] to deconfined quantum critical point and quantum spin liquids with their fractionalized excitations [14, 24].

## Data availability

The data that support the findings of this study are available from the corresponding author upon reasonable request.

## Code availability

All numerical codes in this paper are available upon reasonable request to the authors.

## References

- 
- \* zymeng@hku.hk
- [1] Wen, X.-G. Choreographed entanglement dances: Topological states of quantum matter. *Science* **363**, 864 (2019).
  - [2] Kitaev, A. Yu. Fault-tolerant quantum computation by anyons. *Annals of Physics* **303**, 2 (2003).
  - [3] Tsui, D. C., Stormer, H. L., and Gossard, A. C. Two-Dimensional Magnetotransport in the Extreme Quantum Limit. *Phys. Rev. Lett.* **48**, 1559 (1982).
  - [4] Laughlin, R. B. Anomalous Quantum Hall Effect: An Incompressible Quantum Fluid with Fractionally Charged Excitations. *Phys. Rev. Lett.* **50**, 1395 (1983).
  - [5] Saminadayar, L., Glatli, D. C., Jin, Y., and Etienne, B. Anomalous Quantum Hall Effect: An Incompressible Quantum Fluid with Fractionally Charged Excitations. *Phys. Rev. Lett.* **79**, 2526 (1997).
  - [6] Spånslätt, C., Park, J., Gefen, Y., and Mirlin, A. D. Topological Classification of Shot Noise on Fractional Quantum Hall Edges. *Phys. Rev. Lett.* **123**, 137701 (2019).
  - [7] Banerjee, M., Heiblum, M., Rosenblatt, A., Oreg, Y., Feldman, D. E. and Stern A. Observed quantization of anyonic heat flow. *Nature* **545**, 75 (2017).
  - [8] Wen, X. G. Mean-field theory of spin-liquid states with finite energy gap and topological orders. *Phys. Rev. B* **44**, 2664 (1991).
  - [9] Balents, L., Fisher, M. P. A., and Girvin, S. M. Fractionalization in an easy-axis Kagome antiferromagnet. *Phys. Rev. B* **65**, 224412 (2002).
  - [10] Isakov, S. V., Kim, Y. B., and Paramekanti, A. Spin-Liquid Phase in a Spin-1/2 Quantum Magnet on the Kagome Lattice. *Phys. Rev. Lett.* **97**, 207204 (2006).
  - [11] Isakov, S. V., Hastings, M. B., and Melko, R. G. Topological entanglement entropy of a Bose-Hubbard spin liquid.



- Nature Physics* **7**, 772 (2011).
- [12] Wang, Y.-C., Fang, C., Cheng, M., Qi, Y. and Meng, Z. Y. Topological spin liquid with symmetry-protected edge states. *arXiv e-prints* p. arXiv:1701.01552 (2017).
  - [13] Wang, Y.-C., Zhang, X.-F., Pollmann, F., Cheng, M. and Meng, Z. Y. Quantum spin liquid with even Ising gauge field structure on kagome lattice. *Phys. Rev. Lett.* **121**, 057202 (2018).
  - [14] Sun, G.-Y., Wang, Y. C., Fang, C., Cheng, M., Qi, Y. and Meng, Z. Y. Dynamical signature of symmetry fractionalization in frustrated magnets. *et al.*, *Phys. Rev. Lett.* **121**, 077201 (2018).
  - [15] Samajdar, R., Ho, W. W., Pichler, H., Lukin, M. D. and Sachdev, S. Quantum phases of Rydberg atoms on a kagome lattice. *Proc. Nat. Acad. Sci.* **118**, e2015785118 (2021).
  - [16] Fu, M., Imai, T., Han, T.-H. and Lee, Y. S. Evidence for a gapped spin-liquid ground state in a kagome Heisenberg antiferromagnet. *Science* **350**, 655 (2015).
  - [17] Feng, Z. *et al.* Gapped spin-1/2 spinon excitations in a new kagome quantum spin liquid compound  $\text{Cu}_3\text{Zn}(\text{OH})_6\text{FBr}$ . *Chin. Phys. Lett.* **34**, 077502 (2017).
  - [18] Broholm, C. *et al.* Quantum spin liquids. *Science* **367**, 6475 (2020).
  - [19] Wei, Y. *et al.* Nonlocal effects of low-energy excitations in quantum-spin-liquid candidate  $\text{Cu}_3\text{Zn}(\text{OH})_6\text{FBr}$ . *Chin. Phys. Lett.* **38**, 097501 (2021).
  - [20] Hart, O., Wan, Y. and Castelnovo, C. Correlation holes and slow dynamics induced by fractional statistics in gapped quantum spin. *Natu. Commun.* **12**, 1459 (2021).
  - [21] Beach, K. S. D. Identifying the maximum entropy method as a special limit of stochastic analytic continuation. *arXiv e-prints* p. arXiv:cond-mat/0403055 (2004).
  - [22] Sandvik, A. W. Constrained sampling method for analytic continuation. *Phys. Rev. E* **94**, 063308 (2016).
  - [23] Shao, H. *et al.* Nearly deconfined spinon excitations in the square-lattice spin-1/2 Heisenberg antiferromagnet. *Phys. Rev. X* **7**, 041072 (2017).
  - [24] Ma, N., Sun, G.-Y., You, Y. Z., Xu, C., Vishwanath, A., Sandvik, A. W. and Meng, Z. Y. Dynamical signature of fractionalization at a deconfined quantum critical point. *Phys. Rev. B* **98**, 174421 (2018).
  - [25] Zhou, C. K., Yan, Z., Sun, K., Starykh, O. A. and Meng, Z. Y. Amplitude Mode in Quantum Magnets via Dimensional Crossover. *Phys. Rev. Lett.* **126**, 227201 (2021).
  - [26] Cha, M.-C., Fisher, M. P. A., Girvin, S. M., Wallin, M. and Young, A. P. Universal conductivity of two-dimensional films at the superconductor-insulator transition. *Phys. Rev. B* **44**, 6883 (1991).
  - [27] Damle, K. and Sachdev, S. Nonzero-temperature transport near quantum critical points. *Phys. Rev. B* **56**, 8714 (1997).
  - [28] Chubukov, A. V., Sachdev, S., and Senthil, T. Quantum phase transitions in frustrated quantum antiferromagnets. *Nuc. Phys. B* **426**, 601 (1994).
  - [29] Senthil, T., and Motrunich, O. Microscopic models for fractionalized phases in strongly correlated systems. *Phys. Rev. B* **66**, 205104 (2002).
  - [30] Greiner, M., Mandel, O., Esslinger, T. T. W., Hänsch, T. W. and Bloch, I. Quantum phase transition from a superfluid to a Mott insulator in a gas of ultracold atoms. *Nature* **415**, 39 (2002).
  - [31] Witczak-Krempa, W., Sørensen, E. S. and Sachdev, S. The dynamics of quantum criticality revealed by quantum Monte Carlo and holography. *Nat. Phys.* **10**, 361 (2014).
  - [32] Katz, E., Sachdev, S., Sørensen, E. S. and Witczak-Krempa, W. Conformal field theories at nonzero temperature: Operator product expansions, Monte Carlo, and holography. *Phys. Rev. B* **90**, 245109 (2014).
  - [33] Chen, K., Liu, L., Deng, Y., Pollet, L. and Prokof'ev, N. Universal conductivity in a two-dimensional superfluid-to-insulator quantum critical system. *Phys. Rev. Lett.* **112**, 030402 (2014).
  - [34] Gazit, S., Podolsky, D., Auerbach, A. and Arovas, D. P. Dynamics and conductivity near quantum criticality. *Phys. Rev. B* **88**, 235108 (2013).
  - [35] Gazit, S., Podolsky, D. and Auerbach, A. Critical capacitance and charge-vortex duality near the superfluid-to-insulator transition. *Phys. Rev. Lett.* **113**, 240601 (2014).
  - [36] Chester, S. M. *et al.* Carving out OPE space and precise  $\mathcal{O}(2)$  model critical exponents. *J. Hig. Ener. Phys.* **2020**, 2142 (2020).
  - [37] Sachdev, S. *Quantum Phase Transitions* (Cambridge University Press, 2011), second edn.
  - [38] Myers, R. C., Sachdev, S. and Singh, A. Holographic quantum critical transport without self-duality. *Phys. Rev. D* **83**, 066017 (2011).
  - [39] Witczak-Krempa, W. and Sachdev, S. Quasinormal modes of quantum criticality. *Phys. Rev. B* **86**, 235115 (2012).
  - [40] Fisher, M. P. A. Quantum phase transitions in disordered two-dimensional superconductors. *Phys. Rev. Lett.* **65**, 923 (1990).
  - [41] Herzog, C. P., Kovtun, P., Sachdev, S. and Son, D. T. Quantum critical transport, duality, and M theory. *Phys. Rev. D* **75**, 085020 (2007).
  - [42] Kimchi, I., Nahum, A. and Senthil, T. Valence Bonds in Random Quantum Magnets: Theory and Application to  $\text{YbMgGaO}_4$ . *Phys. Rev. X* **8**, 031028 (2018).
  - [43] Ma, Z. *et al.* Spin-Glass Ground State in a Triangular-Lattice Compound  $\text{YbZnGaO}_4$ . *Phys. Rev. Lett.* **120**, 087201 (2018).
  - [44] Prokof'ev N. V., Svistunov, B. V. and Tupitsyn, I. S. Exact, complete, and universal continuous-time worldline Monte Carlo approach to the statistics of discrete quantum systems. *J. Exp. Theo. Phys.* **87**, 310 (1998).
  - [45] Prokof'ev N. V., Svistunov, B. V. and Tupitsyn, I. S. "Worm" algorithm in quantum Monte Carlo simulations. *Phys. Lett. A* **238**, 253 (1998).
  - [46] Scalapino, D. J., White, S. R. and Zhang, S. C. Superfluid density and the Drude weight of the Hubbard model. *Phys. Rev. Lett.* **68**, 2830 (1992).
  - [47] Anderson, R., Wang, F., Xu, P., Venu, V., Trotzky, S., Chevy, F. and Thywissen, J. H. Conductivity Spectrum of Ultracold Atoms in an Optical Lattice. *Phys. Rev. Lett.* **122**, 153602 (2019).
  - [48] Jo, G.-B., Guzman, J., Thomas, C. K., Hosur, P., Vishwanath, A. and Stamper-Kurn, D. M. Ultracold Atoms in a Tunable Optical Kagome Lattice. *Phys. Rev. Lett.* **108**, 045305 (2012).

## Acknowledgements

We thank Kun Chen, Éric Dupuis, Snir Gazit, Yang Qi, Zhijin Li, David Poland, Subir Sachdev and Erik Sørensen for insightful discussions. YCW acknowledges the supports from the NSFC under Grant No. 11804383, the NSF of Jiangsu Province under



Grant No. BK20180637, and the Fundamental Research Funds for the Central Universities under Grant No. 2018QNA39. M.C. acknowledges support from NSF under award number DMR-1846109 and the Alfred P. Sloan foundation. WWK is funded by a Discovery Grant from NSERC, a Canada Research Chair, a grant from the Fondation Courtois, and a “Établissement de nouveaux chercheurs et de nouvelles chercheuses universitaires” grant from FRQNT. ZYM acknowledges the RGC of Hong Kong SAR of China (Grant Nos. 17303019, 17301420 and AoE/P-701/20)), MOST through the National Key Research and Development Program (Grant No. 2016YFA0300502) and the Strategic Priority Research Program of the Chinese Academy of Sciences (Grant No. XDB33000000). We thank the Computational Initiative at the Faculty of Science and the Information Technology Services at the University of Hong Kong and the Tianhe supercomputing platforms at the National Supercomputer Centers in Tianjin and Guangzhou for their technical support and generous allocation of CPU time.

#### **Author contributions**

M.C., W.W.-K., and Z.Y.M. initiated the work. Y.-C.W. performed the QMC calculations, Y.-C.W. and Z.Y.M. carried out the numerical data analysis. M.C. and W.W.-K. performed the theory analysis. All authors wrote the manuscript together.

#### **Competing interests**

The authors declare no competing interests.

## Supplementary Information for: Fractionalized conductivity and emergent self-duality near topological phase transitions

In this supplementary Information, we present the discussion on the XY\* quantum critical theory, in particular its operator content and the conductivity. We also present the two-step extrapolation of the quantum Monte Carlo data of conductivity from finite sizes and temperatures to the thermodynamic limit, and the fitting of the vison gaps from the imaginary time quantum Monte Carlo data, and their comparison with those obtained from stochastic analytic continuation.

### Supplementary Note 1: XY\* quantum critical theory.

We give a brief summary of the XY\* quantum critical theory, focusing on the operator content in the continuum limit. The QCP is characterized by an emergent conformal symmetry, which means that it is described by a Conformal Field Theory (CFT) in 2 spatial and 1 time dimensions. Let us begin by describing the primary scaling operators in the regular XY (or O(2) Wilson-Fisher) CFT. They are labeled by their charge  $Q$  under the U(1) symmetry. First we discuss scalar (in the Lorentz sense) operators. Numerical conformal bootstrap and  $\epsilon$ -expansion studies give the following values for the scaling dimensions of the first several primary operators [1, 2]:

$$\Delta_{Q=0} = 1.5117, \quad \Delta_{Q=1} = 0.51926, \quad \Delta_{Q=2} = 1.2357, \quad \Delta_{Q=3} = 2.109, \quad \Delta_{Q=4} > 3. \quad (1)$$

The last results two are from  $\epsilon$ -expansion. These correspond to the operator  $O_Q$  with the lowest scaling dimension for the given charge.

We construct the XY\* CFT by coupling the XY CFT to a  $\mathbb{Z}_2$  gauge field, such that only even charges are gauge invariant. Namely, the gauge symmetry is  $(-1)^Q$ . In the new theory, all scalar primaries  $\tilde{O}_Q$  are identified with  $O_{2Q}$  in the XY CFT, which are obviously closed under the Operator Product Expansion (OPE) algebra, and still form a consistent CFT. One must keep in mind that  $\tilde{O}_Q$  still carries physical charge  $Q$ . For example, the charge-1 operator, which is related to  $b^\dagger$  ( $S^+$ ) in the BFG lattice model, has the scaling dimension  $\tilde{\Delta}_1 = \Delta_2 = 1.2357$ , corresponding to the anomalous dimension  $\eta_1 = 2\tilde{\Delta}_1 - 1 = 1.4714$  (reasonably close to the QMC value is 1.53(4) [3, 4]). Interestingly, the minimal (positive) charge is now  $Q = 1/2$ , but the corresponding spinon operator is not gauge invariant. Physically, this tells us that physical states have an even number of spinons.

Now we consider operators with a Lorentz spin of 1 (vectors). Particularly important is the spin-1 current operator  $\tilde{J}_\mu$ . The integrated charge density  $\tilde{J}_0$  inside a closed surface  $\Sigma$ ,  $\tilde{Q}(\Sigma)$ , should satisfy

$$[\tilde{Q}(\Sigma), \tilde{O}_Q] = Q\tilde{O}_Q, \quad (2)$$

when the position of the operator  $\tilde{O}_Q$  is inserted inside the volume enclosed by the surface. Since  $\tilde{O}_Q = O_{2Q}$ , we have

$$[Q(\Sigma), \tilde{O}_Q] = 2Q\tilde{O}_Q. \quad (3)$$

Consistency thus requires that we identify  $\tilde{J}^\mu = \frac{1}{2}J^\mu$ , so  $\tilde{Q} = \frac{1}{2}Q$ . This is expected since the fundamental scalar now carries charge-1/2.

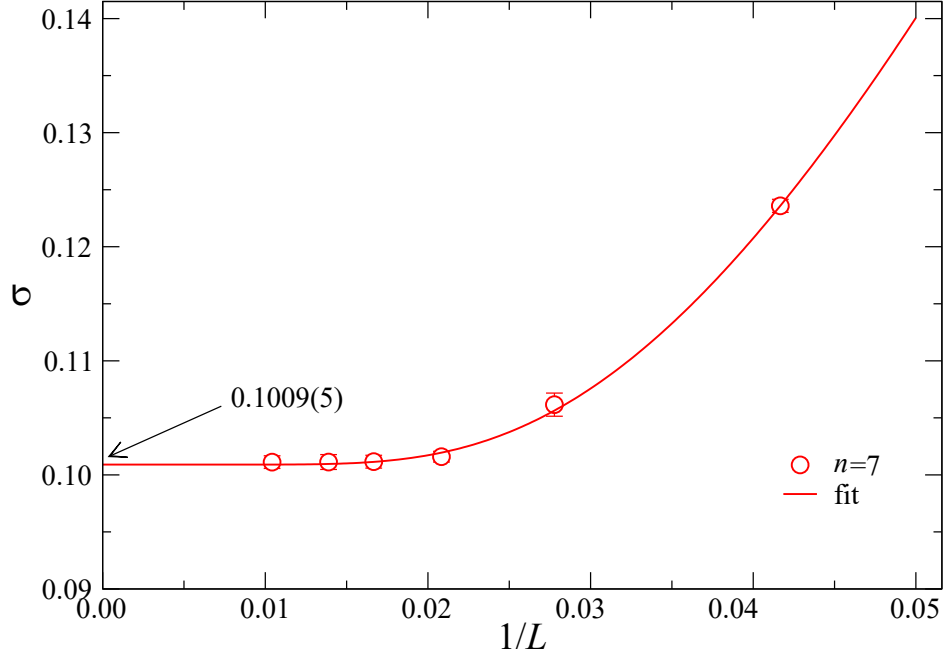
In 2 spatial dimensions, the vacuum two-point correlation function of the current operator is given by (in imaginary time)

$$\langle J_\mu(x) J_\nu(0) \rangle = C_J \frac{\delta_{\mu\nu} - 2\hat{x}_\mu \hat{x}_\nu}{x^4}. \quad (4)$$

Here  $\hat{x}_\mu = \frac{x_\mu}{|x|}$  and  $C_J$  is known as the current central charge. Using Kubo's formula, we can find that  $C_J$  is related to the universal groundstate conductivity by  $\sigma(\infty) = \frac{\pi^2}{2}C_J$ . For the XY CFT, numerical bootstrap yields  $\sigma(\infty) \approx 0.3554$  [5].

### Supplementary Note 2: Extrapolating the conductivity.

In Figs. 2 and 3 of the main text, we show the conductivity results (statistical errors are obtained from QMC simulations and standard data fitting) for inverse temperatures  $\beta V = 300, 350, 390, 400, 450, 500, 520, 550, 600$  with system sizes  $L = 12, 24, 36, 48, 60, 72, 96$  and extrapolate these data to the thermodynamic limit of  $L \rightarrow \infty$  and then  $\beta \rightarrow \infty$ . The extrapolation is rather involved and here we explain the procedure in detail, taking the example of  $\langle n_i \rangle = 1/2$ , while the  $\langle n_i \rangle = 1/3$  results are obtained with the same analysis (statistical errors are obtained using standard data fitting).



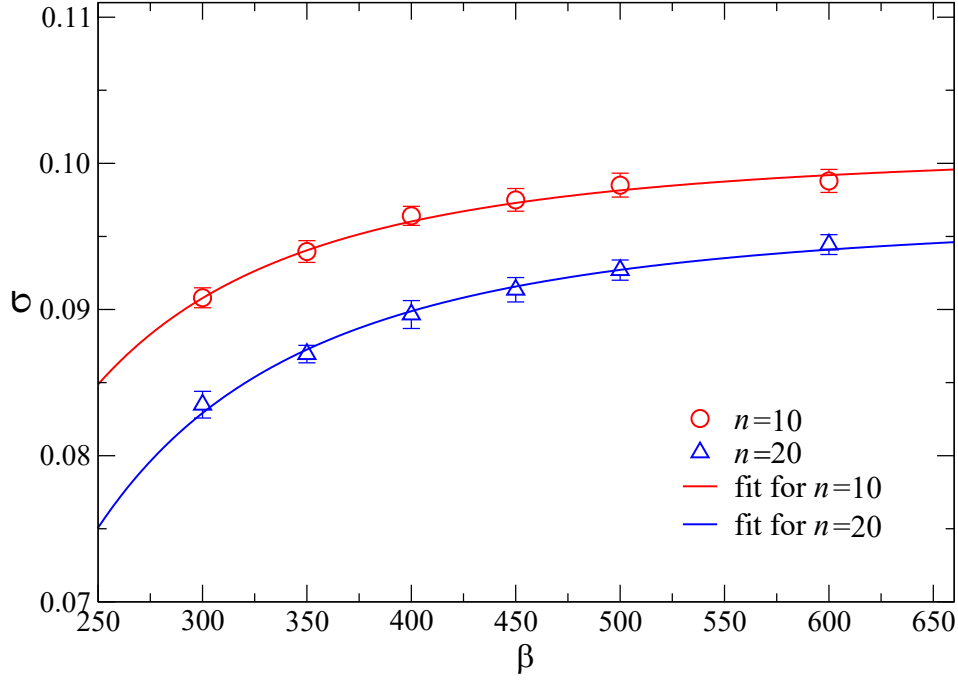
**Supplementary Figure 1. The first step extrapolation of the conductivity.** The conductivity  $\sigma_n$  at  $n = \omega_n/2\pi T = 7$  and boson filling  $\langle n_i \rangle = 1/2$  as a function  $1/L$  with  $\beta V = 500$ . After extrapolation to the thermodynamic limit with the fitting function  $\sigma_n = \sigma_n(L \rightarrow \infty) + b \exp(-L/c)/\sqrt{L}$  (red line), one obtains  $\sigma_n(L \rightarrow \infty, \beta V = 500) = 0.1009(5)$ .

According to the previous analysis of the XY conductivity [6–8], the extrapolation to the thermodynamic shall be taken in two steps: first at a fixed inverse temperature  $\beta$ , one extrapolates the conductivity  $\sigma_n$  at every frequency  $\omega_n$  to the system size  $L \rightarrow \infty$ , i.e.  $\sigma_n(L \rightarrow \infty)$ ; then with the obtained  $\sigma_n(L \rightarrow \infty)$ , one performs the extrapolation of the inverse temperature  $\beta \rightarrow \infty$ , i.e.  $\sigma_n(L \rightarrow \infty, \beta \rightarrow \infty)$ . The obtained conductivity will be the one we use to extract the plateau value  $\sigma(\infty)$  with the scaling function  $\sigma_n(L \rightarrow \infty, \beta \rightarrow \infty) = \sigma(\infty) + b/n^{1.533} + c/n^3$ , where 1.533 comes from  $3 - 1/\nu$  with  $\nu$  being the correlation length critical exponent. It takes the same value at both the XY\* and XY QCPs: 0.67 [2].

The example of the first step extrapolation is shown in Supplementary Figure 1, which is  $\sigma(\omega_n)$  with  $n = 7$  at  $\beta V = 500$ . Following the suggestion in Ref. [6, 7] we measure the conductivity at the configuration sector with no winding in the QMC world-line, in order to reduce the finite size effect. Then with  $L = 12, 24, 36, 48, 60, 72, 96$  one sees that the  $\sigma_{n=7}$  indeed converges to the fixed value with the fitting function  $\sigma_n = \sigma_n(L \rightarrow \infty) + b \exp(-L/c)/\sqrt{L}$ , where  $b$  and  $c$  are fitting parameters [7].  $\sigma_n(L \rightarrow \infty)$  of other frequencies are extrapolated in the same way at this  $\beta$  and we then proceed to the same  $L \rightarrow \infty$  extrapolation for all the inverse temperatures  $\beta V = 300, 350, 400, 450, 500, 600$ .

The obtained  $\sigma_n(L \rightarrow \infty)$  are shown in Fig. 2 of the main text. It is clearly seen that different curves are going towards the same limit as  $\beta$  increases. One interesting observation here is that at low frequencies, i.e.  $n = 1, 2, 3, 4, 5$ , the deviation between  $\sigma_n(L \rightarrow \infty)$  at  $\beta V = 300, 350$  with the lower temperature ones is big. Such nonmonotonous behavior is absent in the same analysis of the XY conductivity. This is due to the fact that at the XY\* transition, the energy spectrum is more complicated than that of the XY transition, in particular with the presence of gapped vison excitations. In the kagome lattice Balents-Fisher-Girvin (BFG) model, previous works reveal that at the XY\* transition where the spinon gap is closed, the vison excitations have a very small gap whose inverse is of the order of  $\sim (V/t_c)^2 \approx 200$  [9]. Such a complication in the spectrum means that the extrapolation of the XY\* data will be more difficult than that of the XY case and one cannot stay at relatively high temperature as in the case of XY transition but have to go significantly below the energy scale of the vison gap.

With such understanding of the complexity, we take the second step extrapolation of the inverse temperature  $\beta$ , mainly using the data of  $\beta V \geq 300$ . The extrapolation at two representative frequencies  $\omega_n$  with  $n = 10$  and 20 are shown in Supplementary Figure 2. Here the extrapolation of  $\beta$  shall also follow a power-law,  $\sigma_n(L \rightarrow \infty) = \sigma_n(L \rightarrow \infty, \beta \rightarrow \infty) + b/\beta^\omega$  [6, 7], where  $\sigma_n(L \rightarrow \infty, \beta \rightarrow \infty)$  is the final extrapolated conductivity at this frequency, and  $b$  is a fitting parameter and the  $\omega$  is an effective exponent taking care of the corrections to the scaling, such scaling analyses have been successfully applied in the previous literatures on the conductivity extrapolation of superfluid-Mott insulator transitions [6–8]. We find that a larger  $\omega = 2.5$  is a good choice such that the fitting curve can go



**Supplementary Figure 2. The second step extrapolation of the conductivity.** Two examples of  $\beta$  extrapolation of  $\sigma_n(L \rightarrow \infty, \beta \rightarrow \infty)$  at  $n = 10$  and  $n = 20$ . The fitting function is  $\sigma_n(L \rightarrow \infty, \beta \rightarrow \infty) = \sigma_n(L \rightarrow \infty, \beta \rightarrow \infty) + b/\beta^\omega$  [6, 7]. We find the effective correction exponent  $\omega = 2.5$  gives the best fit for all the frequencies, when considering the data point  $\beta \geq 300$  to avoid the vison gap. The extrapolated values are  $\sigma_{n=10}(L \rightarrow \infty, \beta \rightarrow \infty) = 0.101(1)$  and  $\sigma_{n=20}(L \rightarrow \infty, \beta \rightarrow \infty) = 0.097(1)$ .

through all the data points at  $\beta V = 300, 350, 400, 450, 500$  and  $600$  for all the frequencies. Note that our choice of  $\omega$  is larger than the effective value of  $\sim 0.9$  used in the XY case, this is again the signature of the complexity of the critical spectra at the XY\* transition. With such power-law form, one obtains  $\sigma_{n=10}(L \rightarrow \infty, \beta \rightarrow \infty) = 0.101(1)$  and  $\sigma_{n=20}(L \rightarrow \infty, \beta \rightarrow \infty) = 0.097(1)$ , as shown in Supplementary Figure 2. We further apply the same procedure for all the frequencies and the obtained  $\sigma_n(L \rightarrow \infty, \beta \rightarrow \infty)$  are shown in Fig. 2 of the main text.

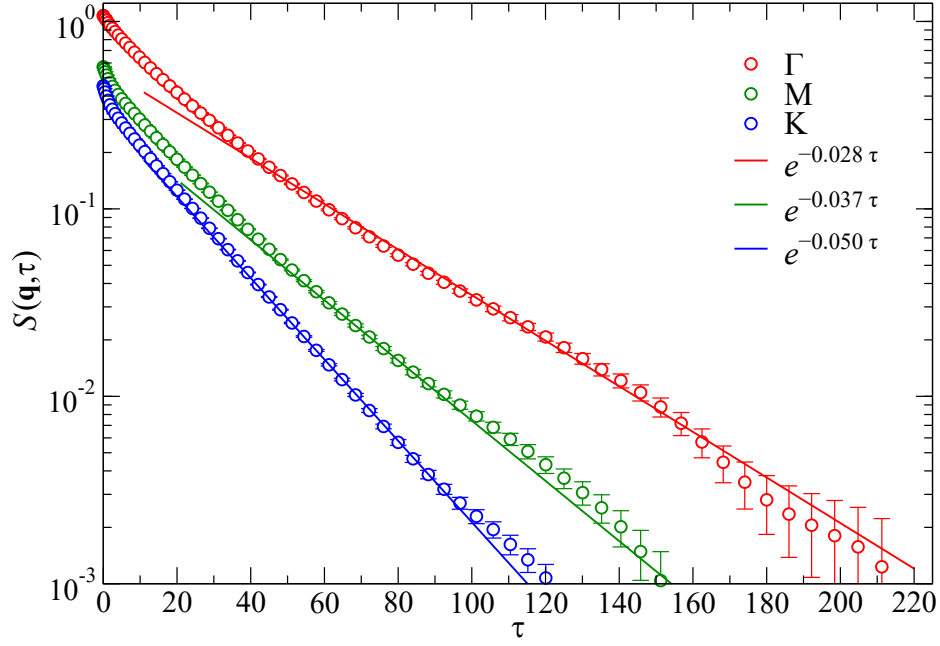
Finally, we fit the data in Fig. 2 of the main text with the scaling function  $\sigma_n(L \rightarrow \infty, \beta \rightarrow \infty) = \sigma(\infty) + b/n^{1.533} + c/n^3$ , with the (2+1)D O(2) correlation length exponent  $\nu = 0.67$  plugged in. By choosing the frequency range of  $n \in [1, 20]$ , we can obtain the plateau value  $\sigma(\infty) = 0.098(9)$  as discussed in the main text, whose value is within error bars 1/4 of the XY  $\sigma(\infty)$ . The coefficients  $b$  and  $c$  are found to depend very sensitively on the range of frequency used in the fit, but the overall sign structure, i.e.  $b > 0$  and  $c < 0$ , is the same as those of the XY case. The ambiguity in  $b$  and  $c$  is likely due to the complex energy spectra at the XY\* transition, especially the presence of the small vison gap. To resolve this issue, one would need to simulate the system at a much lower temperature and with larger system sizes, which are clearly beyond the scope of the current study and actually pose a challenging problem in terms of performing the next-generation QMC simulation schemes. We will leave such tasks to future works with more efficient algorithms and powerful supercomputing platforms.

### Supplementary Note 3: Obtaining the vison gap.

The vison-pair spectra shown in Fig. 4 of the main text are obtained using the QMC-SAC scheme, and we have revealed the gapped spectra at the  $\langle n_i \rangle = 1/2$  and  $\langle n_i \rangle = 1/3$  XY\* transition points. In fact, the presence of the vison gap can be directly read from the raw QMC data of the imaginary time decay of the dynamic spin correlation functions  $S(\mathbf{q}, \tau)$ , which is the spatial Fourier transform of  $\langle S_i^z(\tau) S_j^z(0) \rangle$ .

As shown in Supplementary Figure 3, we present such  $S(\mathbf{q}, \tau)$  at  $\langle n_i \rangle = 1/3$  XY\* transition with  $L = 18$  and  $\beta = 600$  for few representative momenta. The exponential decay can be clearly seen and we fit the vison-pair gap with  $S(\mathbf{q}, \tau) \sim a \exp(-\Delta(\mathbf{q})\tau)$  for the datas of  $\tau \geq 40$  and the gap at different momenta can therefore be fitted.

Since the vison spectra are continua, we find the obtained value of the fitted gap in Supplementary Figure 3 are consistent with those seen in the analytic continued spectrum in Fig. 4(b) of the main text, in that, the fitted values correspond to the position between the lower edge to the brightest spectral weights in the continua. For example, the  $\Delta(\Gamma) \sim 0.028$  and  $\Delta(K) \sim 0.05$ . This is another verification of the robustness of the QMC-SAC scheme employed



**Supplementary Figure 3. Obtaining the vison gap in imaginary time.**  $S(\mathbf{q}, \tau)$  as functions of  $\tau$  at  $\mathbf{q} = \Gamma, M$  and  $q = K$  for the XY\* transition at  $\langle n_i \rangle = 1/3$  case with  $L = 18$  and  $\beta = 600$ . The fitting function is  $ae^{-\Delta(\mathbf{q})\tau}$  (for the datas of  $\tau \geq 40$ ) and the obtained gap are shown in the figure.

here.

---

\* zymeng@hku.hk

- [1] Poland, D., Rychkov, S. and Vichi, A. The conformal bootstrap: Theory, numerical techniques, and applications. *Rev. Mod. Phys.* **91**, 015002 (2019).
- [2] Chester, S. M. *et al.* Carving out OPE space and precise O(2) model critical exponents. *J. Hig. Ener. Phys.* **2020**, 2142 (2020).
- [3] Isakov, S. V., Melko, R. G. and Hastings, M. B. Universal Signatures of Fractionalized Quantum Critical Points. *Science* **335**, 193 (2012).
- [4] Wang, Y.-C., Fang, C., Cheng, M., Qi, Y. and Meng, Z. Y. Topological spin liquid with symmetry-protected edge states. *arXiv e-prints* p. arXiv:1701.01552 (2017).
- [5] Reehorst, M., Trevisani, E. and Vichi, A. Mixed scalar-current bootstrap in three dimensions. *J. Hig. Ener. Phys.* **2020**, 156 (2020).
- [6] itczak-Krempa, W., Sørensen, E. S. and Sachdev, S. The dynamics of quantum criticality revealed by quantum Monte Carlo and holography. *Nat. Phys.* **10**, 361 (2014).
- [7] Chen, K., Liu, L., Deng, Y., Pollet, L. and Prokof'ev, N. Universal conductivity in a two-dimensional superfluid-to-insulator quantum critical system. *Phys. Rev. Lett.* **112**, 030402 (2014).
- [8] Katz, E., Sachdev, S., Sørensen, E. S. and Witczak-Krempa, W. Conformal field theories at nonzero temperature: Operator product expansions, Monte Carlo, and holography. *Phys. Rev. B* **90**, 245109 (2014).
- [9] Sun, G.-Y., Wang, Y C., Fang, C., Cheng, M., Qi, Y. and Meng, Z. Y. Dynamical signature of symmetry fractionalization in frustrated magnets. *et al., Phys. Rev. Lett.* **121**, 077201 (2018).